# Journal of Materials Chemistry B

Accepted Manuscript






ROYAL SOCIETY OF CHEMISTRY

www.rsc.org/materialsB

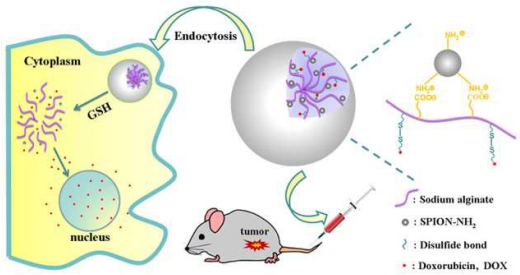


DOX anchored via disulfide onto algiate coated superparamagnetic nanoparticles promised high efficacy with low systemic adverse effect.

# Redox stimuli-responsive superparamagnetic nanogel with chemically anchored DOX for enhanced anticancer efficacy and low systemic adverse effect

Lidi Chen[1], Yanan Xue[1], Xiaoyang Xia[1], Meifang Song[1], Juan Huang[1], Han Zhang[1], Bo Yu[1], Sihui Long[1], Yanping Liu[1], Lei Liu[2], Shiwen Huang[2], Faquan Yu[1, *]

[1] *Key Laboratory for Green Chemical Process of Ministry of Education*

*Hubei Key Laboratory for Novel Reactor and Green Chemistry Technology*

*School of Chemical Engineering and Pharmacy,*

*Wuhan Institute of Technology, Wuhan 430073, China*

[2] *College of Chemistry and Molecular Sciences*

*Wuhan University, Wuhan 430072, China*

[*]Corresponding author:

Faquan Yu, Professor, PhD

Wuhan Institute of Technology

Xiongchu Ave, Wuhan 430073, Hubei, China

E-mail address: fyu@wit.edu.cn; fyuwucn@gmail.com

Tel: (86-27) 8719-4980; Fax: (86-27) 8719-4465

## Abstract

A reduction-triggered superparamagnetic nanogel was designed for enhancing targeting release but minimizing leakage of drug on the drug-transportation pathway. Doxorubicin (DOX) was first conjugated onto sodium alginate (SA) with disulfide linker (SA-SS-DOX). SA-SS-DOX was then electrostatically assembled with aminated superparamagnetic iron oxide nanoparticles for the preparation of nanogel. The nanogel was estimated with a size of 122±15 nm, a polydispersity index of 0.178, surface charge of around -36.0 mV, DOX loading of 7.2 wt%, and saturation magnetization of 40.0 emu/g Fe. *In vitro* release profiles showed a significantly high accumulative release at pH 5.5/10 mM Glutathione (GSH) but pretty low release at pH 7.4/pH 5.5 without GSH, exhibiting apparent reduction responsiveness. *In vitro* cytotoxicity tests clearly illustrated the effective selectivity of killing the human cervical cancer cells (HeLa) with $IC_{50}$ of 0.30 μg/mL, significantly enhanced the cytotoxicity of the african green monkey Sv40-transformed kidney fibroblast cells (COS-7). Prussian blue staining and quantification of cellular iron and protein concentration revealed apparent iron uptake by HeLa cells. Confocal laser scanning microscopy observation demonstrated that DOX was efficiently internalized into HeLa cells, released into the cytoplasm, and then principally entered the nuclei. *In vivo* investigation exhibited that the nanogel treatment induced obvious shrinkage in tumor volume but a stable growth in body weight and a healthy appearance. Hematoxylin-eosin (H & E) staining indicated remarkable necrosis in the tumor area and histologic examination revealed the lower toxicity in vital organs. Thus this kind of nanogel expressed high targeted release but low systemic toxicity. It is thus believed that this nanogel will offer a promising candidate for highly effective cancer therapy.


**Keywords**: alginate, reduction-responsiveness, conjugate, nanogel

## 1. Introduction

In past decades, anti-cancer drug delivery systems have attracted much attention.[1-3] Great effort has been directed to the development of preferential accumulation and specific release of anticancer agents at target sites for enhancing therapeutic efficacy and minimizing the release or leakage during the transportation of the vehicles toward to the area of interests for low systemic side effect.

Superparamagnetic nanoparticles (SPION) as a drug vehicle are a preferential platform for the drug accumulation at target sites by taking advantage of the magnetic mobility evoked by external magnetic field.[4,5] This has been documented widely.[2,5] Moreover, SPION have additional functions such as magnetic thermotherapy (hyperthermia) and magnetic resonance imaging (MRI)[6]. Therefore, SPION are investigated as a drug carrier experimentally and clinically.[2,7]

To achieve specific release at targeting regions, numerous researches have been done to develop stimuli-responsive drug carriers.[3,8] Tumor intracellular environment exhibits the concentration of 1-10 mM glutathione (GSH), which is much times higher than that in the extracellular circulation and fluids (~2 μM).[9] The significant difference in reductive potential has been employed to achieve

reduction-triggered drug release.[8] Disulfide bond is such a linkage that is easy to break down under reduction potential environment.[10] Nanogels crosslinked via disulfide bond were frequently served as the vehicle to achieve the goal in that the nanogel would be stable in the blood circulation and be broken when it reached the tumor tissue, releasing the embedded drug such as DOX.[11-13] However, in some cases, near a half of the final release amount was documented without any reductive stimulus.[14,15] This will inevitably lead to leaching of DOX during the transportation and thus systemic adverse effect. The reason is presumably that there is a paucity of strong interaction between the physically embedded DOX with the nanogel though the latter was a crosslinked network matrix.

Improvements are still required in designing a stimuli-responsive system. Chemical conjugation of drug with the nanogel is a preferential option to immobilize drug tightly inside the nanogel. In fact, there are some reports pertinent to the covalent conjugation of anticancer drugs with polymeric chain via cleavable hydrazone,[16] ester,[17] disulfide[10] and other biologically responsive bonds[18,19] for the purpose of enhanced stability of prodrugs.

Previously, the incorporation of redox stimuli triggered release with magnetic nanoparticles has been designed[20,21] for this purpose of targeted accumulation and specific release. The drug DOX, however, was simply encapsulated into the nanogel. As above, this type of nanogel structure exhibits a dramatic initial burst release.

Obviously, it is advantageous to develop a superparamagnetic nanogel with covalently bonded DOX in enhanced accumulation at site of targets and reduced chance of leakage in the delivery pathway. In this study, a superparamagnetic nanogel was prepared, where DOX was chemically anchored onto the nanogel matrix via disulfide bond. By virtue of the mechanism of the least leakage during the transportation and the preferential accumulation at diseased sites, the so-prepared nanogel is expected to feature as the effective efficacy and obvious low adverse systemic effect.

## 2. Experimental section

### 2.1 Materials

All chemical reagents were used as received. Sodium alginate (SA, Mw= 32-250 kDa) and N-(3-dimethylaminopropyl)-N'-ethylcarbodiimide hydrochloride (EDC·HCl, 98.5%) were purchased from Aladdin. Cysteamine hydrochloride (99%), N-hydroxysuccinimide (NHS), glutathione (GSH), 3-mercaptopropionic acid (MPA, >99%), 5,5'-dithiobis (2-nitrobenzoic acid) (DTNB, 95%), glycine (98.5%), iron(II) chloride tetrahydrate ($FeCl_2 \cdot 4H_2O$, 98%), iron(III) chloride hexahydrate ($FeCl_3 \cdot 6H_2O$, 97%), dimethyl sulfoxide (DMSO), sodium hydroxide (NaOH), sodium chloride (NaCl) and hydrogen peroxide ($H_2O_2$, 30%) were purchased from Sinopharm Chemical Reagent. Doxorubicin hydrochloride (DOX·HCl, >98%) was purchased from Dalian Meilun Biology Technology Co.Ltd. Fluoresceinamine isomer (≥95%), potassium hexacyanoferrate (II) trihydrate ($K_4[Fe(CN)_6] \cdot 3H_2O$, ≥98.5%), potassium thiocyanate (KSCN, ≥99%), paraformaldehyde (95%), Hoechst 33258, and 3-[4,5-dimethylthiazol-2-yl]-2,5-diphenyltetrazoplium bromide (MTT) were purchased from Sigma-Aldrich. Dimethyl sulfoxide-*d6*

(DMSO-*d6*) was purchased from Cambridge Isotope Laboratories. Ultrapure water was prepared by Heal Force super NW water purification system (Heal Force Development Ltd.). Glycine-modified superparamagnetic iron oxide nanoparticles (SPION-$NH_2$) were synthesized following a co-precipitation method.[22-23] COS-7, HeLa, H22 cell lines were purchased from Chinese Typical Culture Center (CTCC, Wuhan University) and cultured in RPMI-1640 medium (Gibco) supplemented with 10% fetal bovine serum (FBS, Hyclone) and 1% antibiotics (100 U/mL penicillin and 100 mg/mL streptomycin) at 37 °C in a humidified atmosphere containing 5 % $CO_2$.

**2.2 Characterization**

The FTIR spectra were recorded with a Nicolet 5700 spectrometer in the wavenumber range of 400-4000 $cm^{-1}$. UV-vis spectra and fluorescence spectra were recorded using a Hitachi fluorescence spectrophotometer-F-4600 at room temperature. $^1H$ nuclear magnetic resonance ($^1H$ NMR) spectra were recorded on a Bruker Avance-500 spectrometer using DMSO-*d6* as a solvent. The size, size distribution, and zeta potential were investigated by dynamic light scattering (DLS) and electrophoresis, respectively, using a Zetasizer (Malvern Nano-ZS90) with a He-Ne laser beam at 633 nm at 25 °C. The morphology of the nanogel was observed at Tecnai G2S-Twin TEM at an accelerating voltage of 200 kV. Magnetization measurements were obtained on a vibrating-sample magnetometer (VSM, Westerville, OH, USA) via changing the magnetic field from -15,000 to 15,000 Oe at 25 °C.

**2.3 Synthesis of thiolated alginate (SA-SH)**

SA-SH was synthesized by an amidation process following a literature with a slight modification.[24] Briefly, 0.50 g alginate was dissolved in 30 mL ultrapure water under magnetic stirring for 2 h. To this solution 0.96 g EDC·HCl was added. After stirring for 45 min, 0.58 g NHS was added and the system was stirred for another 45 min. Thereafter, 0.52 g cysteamine hydrochloride was added to the above solution. Then pH was adjusted to 5 using 1 mol/L NaOH solution. The reaction mixture was stirred for 12 h under nitrogen protection and in dark environment. All these processes were at room temperature. Finally, the resultant solution was dialyzed against ultrapure water and lyophilized. The product obtained was stored at 4 °C until further use.

The amount of thiol group was estimated by a colorimetric method using Ellman's reagent (DTNB).[25] Briefly, 50 µL Ellman's reagent solution (0.01 mol/L) in PBS (0.1 mol/L, pH 8.0) and 50 µL sample suspension were hydrated in 2.5 mL PBS in sequence. After incubation for 30 min at room temperature, the absorbance of the samples at 410 nm wavelength was monitored, with water instead of the sample solution as blank. The amount of thiol groups was calculated using a calibration curve obtained from cysteine.

**2.4 Synthesis of the conjugate of alginate with doxorubicin via disulfide bond (SA-SS-DOX)**

SA-SS-DOX was synthesized using a following reaction procedure. DOX was thiolated first via the amidation with 3-mercaptopropionic acid. Briefly, 28.7 mg EDC·HCl was dissolved in 10 mL ultrapure water. Then 1.3 µL 3-mercaptopropionic acid

was added to the EDC·HCl solution under stirring in anaerobic dark environment. After 45 min, 17.3 mg NHS was added and stirred for another 45 min. 8.7 mg DOX·HCl was dissolved in 12.2 mL ultrapure water and added dropwise into the above solution. Then pH was adjusted to 5 using 1 mol/L NaOH solution. The thiolation proceeded for 12 h. Subsequently, 20 mg SA-SH was dissolved in 13.7 mL ultrapure water and added dropwise. After mingled well, 0.15 mL $H_2O_2$ (1 mol/L in $H_2O$) was added into the mixture. To remove the non-chemically bonded DOX thoroughly, the product SA-SS-DOX was dialyzed (MWCO 14000) against HCl (pH 5.5) until no DOX was detected in dialysis fluid (4 shifts) and finally against ultrapure water (2 shifts).

To check the successful synthesis of DOX-SH, the crude product of DOX-SH was purified by column chromatography using silica gel as the stationary phase and a mixture of methanol/ethyl acetate(1/9, v/v) as a mobile phase to obtain pure DOX-SH for further characterization.

**2.5 Preparation and fluorescence labeling of magnetic DOX-anchored nanogel (MDAN-gel)**

The MDAN-gel was prepared by virtue of the electrostatic interaction between the left carboxyl groups of SA and the amino groups of SPION-$NH_2$. 6 mL SA-SS-DOX (0.5 mg/mL) was loaded into a three-neck flask and pH was adjusted to 5.0 by using HCl. 4.0 mL SPION-$NH_2$ suspension (1.5 mg /mL, pH 5.0) was added dropwise to the SA-SS-DOX solution. Afterwards, the pH of the mixture solution was increased slowly to 7.4 with 0.1 mol/L NaOH, resulting in the MDAN-gel. The nanogel was then labeled with fluoresceinamine isomer according to the method published previously.[26,27] Plain nanogel or DOX-free nanogel was prepared following the above procedure with the exception of the replacement of SA-SS-DOX by SA-SH.

**2.6 *In vitro* release of DOX**

The DOX release studies were performed under different pHs and GSH concentrations. 2 mL of the MDAN-gel suspension prepared above was loaded into dialysis tube (MWCO 3500) and then immersed into 8 mL 0.01 mol/L PBS of pH 5.5 or pH 7.4 with GSH. The final GSH concentration was set at 0, 2 μM or 10 mM, respectively. All the tests were conducted in a water bath with shaking rate at 60 rpm at 37 °C. 1 mL of the incubation medium was taken out every 2 h and 1 mL of the corresponding fresh medium was refilled to maintain the volume, pH and GSH concentration. The amount of released DOX was determined in light of the fluorescent analysis by measuring the excitation at 480 nm and emission at 590 nm using a calibration curve prepared previously under the corresponding conditions. All measurements were performed in triplicate. Drug loading content (DLC) and drug entrapment efficiency (DEE) were defined as follows:

$$\text{Drug loading content}\,(\%) = \frac{W_{drug}}{W_{MDAN\text{-}gel}} \times 100\ \%$$

$$\text{Drug entrapment efficiency}\ (\%) = \frac{W_{drug}}{W_{fed\ drug}} \times 100\ \%$$

Where $W_{MDAN\text{-}gel}$ is the weight of lyophilized nanogel, including the anchored DOX, $W_{drug}$ was the weight of DOX in the nanogel,

which was calculated as the total released weight of DOX from nanogel, and $W_{fed\ drug}$ was the fed weight of DOX.

### 2.7. *In vitro* cytotoxicity assay

The cytotoxicity of the MDAN-gel and free DOX against HeLa cells and COS-7 cells was evaluated using MTT assay. Cells were seeded into a 96-well plate at a density of ~5000 cells per well in 100 μL complete RPMI 1640 medium containing 10% FBS and cultured for 1 day at 37 °C in 5% $CO_2$ atmosphere. Then, 100 μL MDAN-gel (including plain nanogel) or DOX (including DOX-SH) that was serially diluted in complete RPMI 1640 medium at different concentrations ranging from $1.0\times10^{-4}$ mg/mL to $7.7\times10^{-2}$ mg/mL and from $4.0\times10^{-2}$ μg/mL to 5.0 μg/mL, respectively, was separately loaded into wells. As a control, 100 μL solution of fresh complete RPMI-1640 medium without any MDAN-gel or DOX was applied. After 48 h incubation, the culture medium was disposed and the cells were washed thrice with PBS. Subsequently, 100 μL culture medium and 20 μL of MTT (5 mg/mL) solution was added and incubated for 4 h. The medium was carefully removed, and 150 μL DMSO was added into each well to dissolve the formazan crystals. In the above procedure, blank wells were designed by substituting PBS solution for MTT solution. The absorbance of the solution in well at 570 nm was measured using a microplate reader (Macromolecule Devices SpectraMax M2e). The percent relative cell viability in reference to control wells was calculated by the following equation:

$$\text{Relative cell viability (\%)} = \frac{A_{sample} - A_{blank}}{A_{control} - A_{blank}} \times 100\ \%$$

Relative cell viability graphs were plotted against DOX concentrations for convenient comparison. Data were presented as average ± SD (n = 8).

### 2.8. Cellular uptake

#### 2.8.1. Prussian blue staining

Prussian blue staining was used as a qualitative and visual method to observe the intracellular iron distribution.[20] HeLa cells were seeded into a 24-well plate at a density of ~5 x $10^4$ cells per well in 1 mL complete RPMI-1640 medium containing 10% FBS and cultured for 1 day at 37 °C in 5% $CO_2$ atmosphere. Then, the culture medium was replaced with 1 mL of fresh medium containing 198 μg/mL plain nanogel. The control sample was designed while no nanogel was applied. The cells were washed thrice with PBS (0.01 mol/L, pH 7.4) after incubation for 24 h, and then fixed for 10 min using 4% (w/v) paraformaldehyde. The cells were washed thrice with PBS and stained with 1 mL freshly prepared 4% potassium ferrocyanide and 8% HCl solution for 30 min at 37 °C. Finally, the stained cells were visualized by a reverse microscope (Ti, Nikon, Japan) after three washes with PBS.

#### 2.8.2. Confocal laser scanning microscopy (CLSM) observation

CLSM was employed to visualize the intracellular distribution of DOX. HeLa cells were seeded in the culture dish with a coverslip at a density of ~$2\times10^5$ cells per well and cultured for 1 day. The cells were then incubated with MDAN-gel for 4 h or 24 h at 37 °C. The final concentration of MDAN-gel was 6.94 μg/mL. At predetermined interval, the culture media was subsequently removed and the cells were washed thrice with PBS and fixed with 4% (w/v) paraformaldehyde for 10 min at room temperature. The slides were then rinsed thrice with PBS. Finally, the cells were stained with Hoechst 33258 (5 mg/mL in PBS) at 37 °C for 10 min. After further rinsed with PBS thrice, the prepared slides were examined by CLSM (Nikon, TE2000, EZ-C1, Japan).

### 2.9. *In vivo* antitumor efficacy

All animal experiments were performed in compliance with the guidelines approved by the committee of Wuhan University on Use and Care of Animals. The tumor growth inhibitory activities were assessed in BABL/c mice (female 5-6 weeks old, animal experiment center of Wuhan university, China). The H22 mouse liver cancer cells ($1\times10^7$ cells/mL, 0.1 mL) were implanted in the femoribus internus. When tumors grew to an average volume of about 100 $mm^3$, the mice were randomly divided into three groups (n=4), and intravenously administered via tail vein weekly with sterile PBS, DOX·HCl, and MDAN-gel, respectively, at a dose of 10 mg (DOX)/kg (body weight). The body weight and tumor volume were followed every two days. All mice were sacrificed on the day 21. The tumor size was estimated with a caliper in two dimensions and calculated.[28] The tumor size was expressed as an arithmetic means with a standard error. The inhibition rate of tumor growth was calculated as follows:

$$\mathrm{IR}(\%) = 1 - \frac{\text{weight of tumor in experimental group}}{\text{weight of tumor in control group}} \times 100\%$$

### 2.10. Histological analyses

The tumors and major organs (heart, liver, spleen, lung and kidney) were excised, weighed, and then fixed in 4% PBS buffered paraformaldehyde overnight, and then embedded in paraffin. The paraffin embedded tumors and organs were cut at 5 μm thickness, and stained with hematoxylin-eosin (H&E) and with prussian blue for pathological examination and histological alterations assessment by microscope (OLYMPUS IX51 / Q-IMAGING Micro Publisher).

## 3. Results

Scheme 1 depicts the fabrication of the MDAN-gel and the stimulus-responsive release of drug in cancerous cells. Sodium alginate (SA) was chosen as the principal biomacromolecule for the fabrication of nanogel by virtue of the affluent carboxylic groups. The carboxylic groups were partially transferred into thiol groups (SA-SH), in one respect. The subsequent conjugation of SA-SH with previously thiolated DOX (DOX-SH) formed disulfide bond upon the oxidation between thiol groups under the action of peroxide

hydrogen. The bond functions as the cleavable linkage for the achievement of the reduction responsiveness of release. In another respect, aminated magnetic nanoparticles (SPION-$NH_2$) were previously prepared following literatures.[22] The left carboxylic groups on SA were employed to combine with the amine groups through electrostatic interaction. Upon the optimized ratio of SA-SH to DOX-SH or to SPION-$NH_2$, the nanogel can be obtained in an appropriate size. The fabricated superparamagnetic nanogel will behave reduction-stimuli responsiveness. These features were evaluated and verified *in vitro* and *in vivo*.

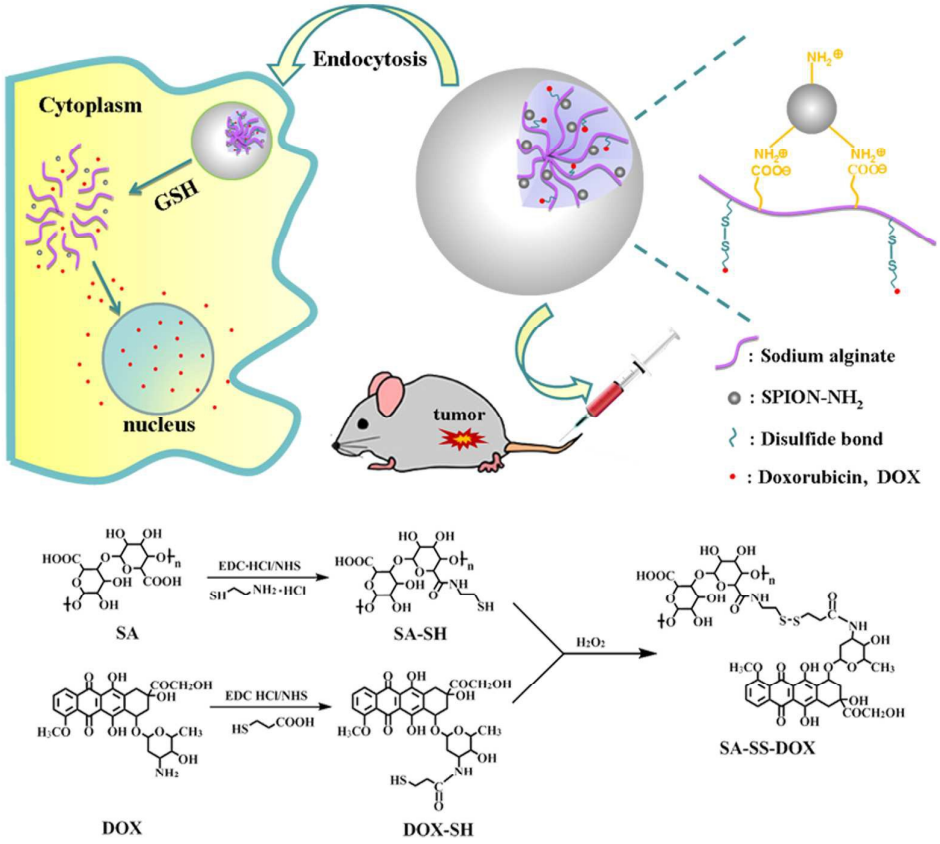


**Scheme. 1.** The synthesis process of SA-SS-DOX, the formation of magnetic DOX-anchored nanogel and the schematic illustration of cellular internalization and triggered intracellular drug release.

### 3.1. Characterization of MDAN-gel

#### 3.1.1. Characterization of thiolated alginate (SA-SH), thiolated doxorubicin (DOX-SH) and SA-SS-DOX

Thiolated alginate (SA-SH) was synthesized by virtue of the amidation between the carboxylic group of alginate and the primary amino group of cysteamine. The FTIR spectrum of SA-SH is shown in contrast with that of SA in Figure 1. The spectrum of SA was found to be in agreement with the previous report.[29] SA-SH shows new peaks at 1700 $cm^{-1}$, 1568 $cm^{-1}$ and 1282 $cm^{-1}$, which are not present in native alginate. These peaks were assigned to amid I, II and III bands, respectively. A weak peak located at 2538 $cm^{-1}$ was believed to belong to the thiol functional group.[24] These exhibited the occurrence of amidation, as anticipated. On the other hand,

the Ellman's test was conducted to quantitatively determine the amount of thiol groups introduced in the thiolation process. It was found that the content of thiol groups is approximately 0.68 mmol/g SA. In another word, the degree of thiolation was calculated to be 12.5% based on the content of carboxylic groups.

The successful synthesis of thiolated doxorubicin (DOX-SH) was confirmed by FTIR and $^{1}$H NMR. As shown in FTIR spectrum (Figure 1), the appearance of a peak at 1640 $cm^{-1}$ (C=O) in DOX-SH and the disappearance of the two peaks at 1583 $cm^{-1}$and 1616 $cm^{-1}$ (N-H), which exist in doxorubicin (DOX), verified the successful thiolation of doxorubicin. The peak at 1207 $cm^{-1}$ (C-O-C asymmetric stretching vibration) in DOX was observed in the spectrum in DOX-SH with a little red shift to 1213 $cm^{-1}$. In light of $^{1}$H NMR shown in Figure 2, the peaks h and i appearing at respective 3.09 and 2.83 ppm were attributed to two methine protons. Their integral ratio was estimated to be 1:1.08. Both the peaks do not exist in the NMR of DOX. These observations indicated the occurrence of the coupling of 3-mercaptopropionic acid and doxorubicin and the successful incorporation of thiol group into DOX.

The formation of SA-SS-DOX was confirmed by both FTIR and UV-vis investigation. SA-SS-DOX still holds these characteristic peaks inherited from DOX-SH at 1213 $cm^{-1}$(C-O-C asymmetric stretching vibration), at 1700 $cm^{-1}$ (amide I band) and at 1290 $cm^{-1}$ (amide III band) (Figure 1). UV-vis spectra of DOX, SA, SA-SS-DOX, and the mixture of DOX and SA were scanned, shown in Figure 3a. The mixture of DOX and SA revealed their overlap spectrum. However, SA-SS-DOX displayed 10 nm of red shift in the maximum absorption position, compared with DOX and with the mixture of DOX and SA, which is in accordance with the previous work.[30,31] All the observation confirmed the successful conjugation of DOX with SA.

In order to comform the thiolate modify has no effect to the measurement DOX in subsequent experiment. The DOX, DOX-SH and SA-SS-DOX water solution (at the same concentration of DOX) were monitored by fluorescence spectrometer at same excitation wavelength (480nm). As shown in Figure 3b, no shift appeared in DOX and DOX-SH, especially at the characteristic peak. It also had been proved in many other work that the spectral characteristics of DOX would not be affected by the short thiol.[30]

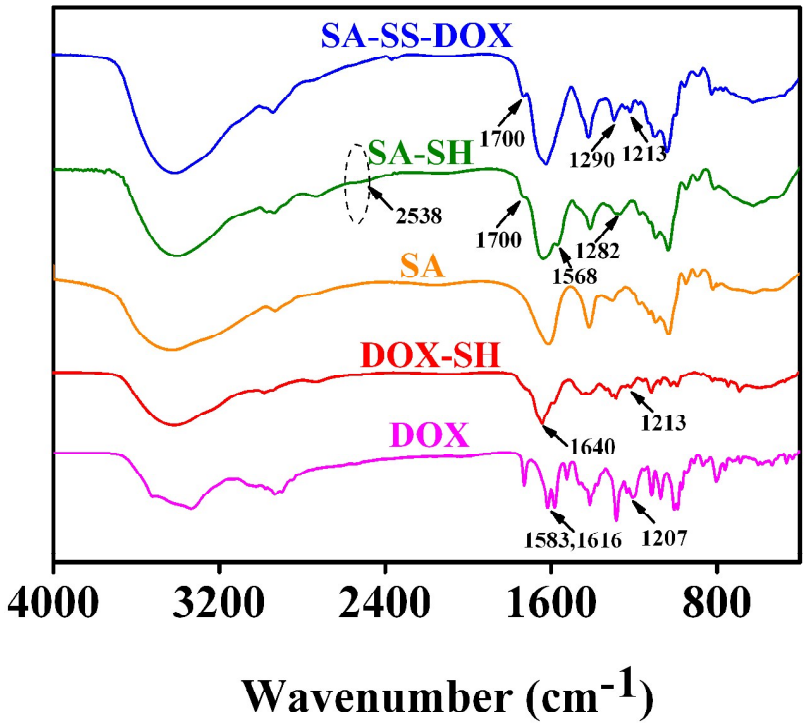


**Figure. 1.** FTIR spectra of doxorubicin (DOX), DOX-SH, alginate (SA), thiolated alginate (SA-SH) and disulfide bond conjugate (SA-SS-DOX)

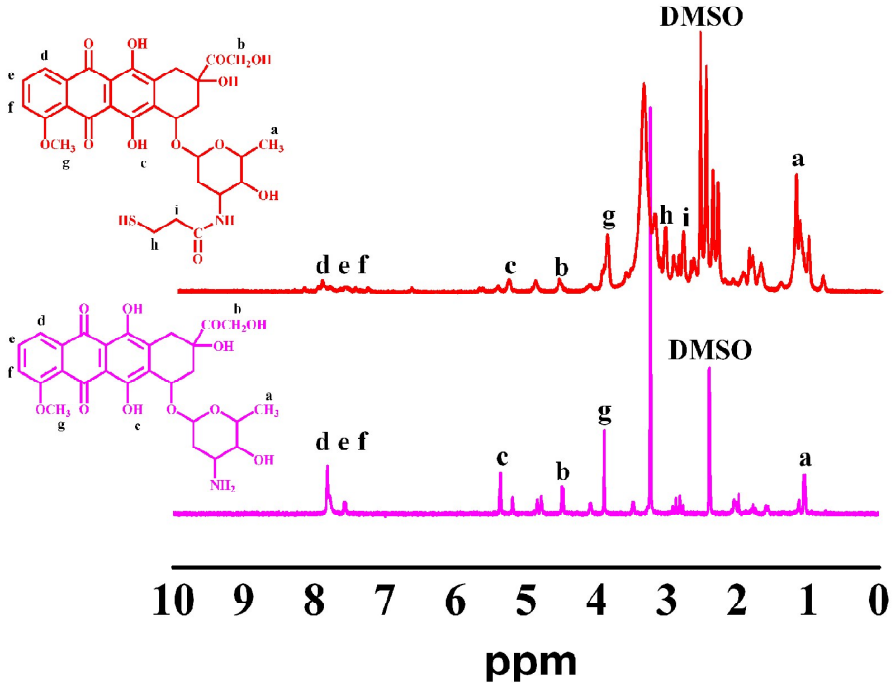


**Figure. 2.** $^{1}$H NMR spectra of DOX and DOX-SH using DMSO-*d6* as a solvent.

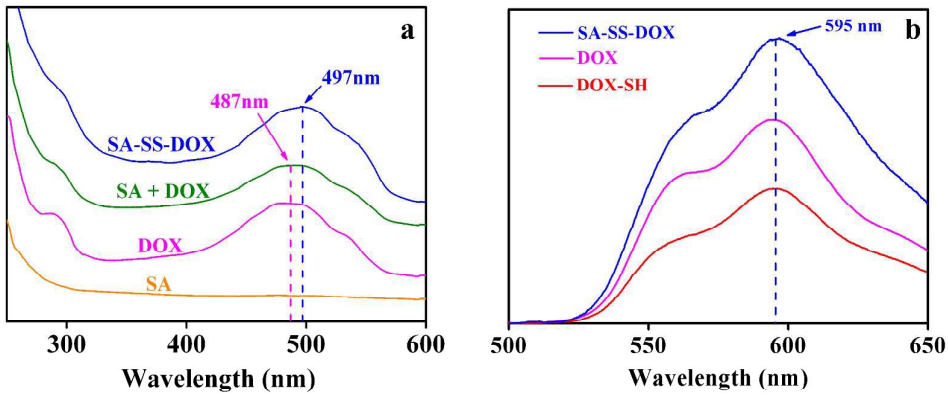


**Figure. 3.** (a) UV/Vis spectra of alginate (SA), doxorubicin (DOX), mixture of alginate and doxorubicin (SA+DOX) and the conjugate of SA and DOX (SA-SS-DOX). (b) Emission spectra of doxorubicin (DOX), thiolated doxorubicin (DOX-SH), and the conjugate of SA and DOX (SA-SS-DOX).

### 3.1.2 Characterization of MDAN-gel

The morphology of the MDAN-gels was observed under TEM directly (Figure 4a). The images indicated that the nanogel contained many small and dark particles. These particles were believed to be SPION, which were densely packed together with SA as the matrix. The irregular morphology is in agreement with previous observation.[32,33] TEM images illustrated that the size was consistent with the result of DLS, shown in Figure 4 b. The average size is approximately 122±15 nm with a polydispersity index of 0.178, indicating a narrow size distribution. As widely known, EPR effect is an unique phenomenon only occurred in tumor tissue. In order to get sufficient supply of nutrients and oxygen for rapid growth, tumor vessels became sparse that the "large" size particle could freely enter and accumulate in tumor tissues.[34] Furthermore, following systemic administration, particles with diameter greater than 200 nm are usually sequestered by spleen as a result of mechanical filtration and are eventually removed by the cells of the phagocyte system, resulting in decreased blood circulation time. On the other hand, smaller particles with diameters of less than 10 nm are rapidly removed through extravasations and renal clearance.[35] In conclusion, the present size and distribution is ideal for the drug delivery carrier taking advantage of EPR effect. As a matter of fact, in order to make the size in this range, a series of weight ratio of SA-SS-DOX over SPION-$NH_2$ were optimized. 2:1 of the ratio was optimized for the subsequent experiments. Additionally, the zeta potential of the nanogel was determined at -36.0±0.9 mV by electrophoresis. When DOX was conjugated onto SA, not all carboxylic groups were occupied. The left carboxylic groups account for the negative surface charge on the nanogel. As well, the sufficient negative charge stabilized the nanogel and provided hydrophilic surface to evade the uptake of reticuloendothelial system (RES). Moreover, the crosslinking of the thiol groups between SA-SH due to the usage of excess hydrogen peroxide will further enhance the stability of the nanogel under physiological conditions with the high level of salt content.

Figure 4c showed the stability of the MDAN-gel in 0.01M PBS buffer containing 0.15 mol/L NaCl at pH 7.4. No significant size increase occurred in 24 hours since the nanogels was dispersed in that medium. No flocculation or precipitate was observed visually. That period of time is much longer than the circulation life of convenient drug delivery carriers and is enough for that nanogel to be targeted. These features make the biological applications feasible.

Due to the incorporation of SPION, the MDAN-gel was anticipated to have the properties of magnetophoresis to an external magnetic field. Figure 4d displayed the visual migration in color after exposed to a magnet. It was observed that dark particles were gradually enriched at the site of the magnet with the prolongation of exposure time. The suspension fluid changed in color from dark (0 h) to brown (24 h) to almost colorless (48 h) at corresponding time intervals. This experiment proved the magnetic responsiveness of the nanogel.

The quantitative measurement of superparamagnetism against applied magnetic field (H) was performed by using VSM, shown in Figure 4e. The free SPION-$NH_2$ and nanogel exhibited superparamagnetic properties, without any remnant hysteresis loop observed. The saturation magnetism was respectively estimated to be 43.1 and 40.0 emu/g Fe. This property indicates that nanogel will migrate in an external magnetic field. In addition, when removed out of external magnetic field, the magnetic interaction among nanogels will disappear completely. The feature will therefore eradicate the potential agglomeration of nanogels, which would, otherwise, induce the thrombosis of blood vessels. These advantages allow the nanogel a high promising candidate as magnetic targeting in drug delivery system.

As well, DLC and DEE were determined at 7.2% and 54.7%, respectively. These were useful to determine the experimental conditions in cell and animal studies.

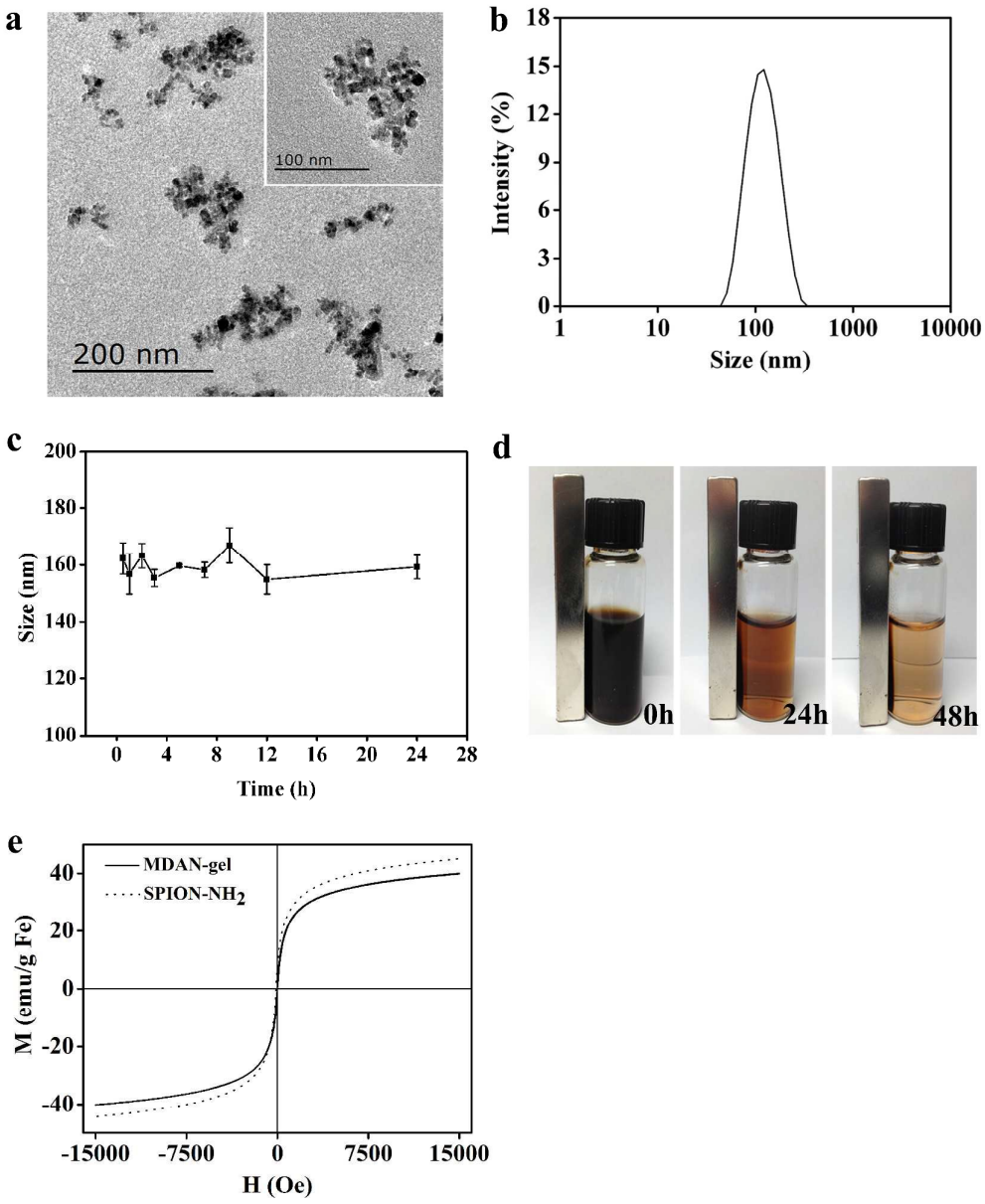


**Figure. 4.** The TEM images (a), the size distribution by DLS (b), the stability of the MDAN-gel in 0.01M PBS buffer containing 0.15 mol/L NaCl at pH 7.4 (c), visual observation of magnetophoresis exposed to a magnet for 0 h, 24 h and 48 h (d), and vibrating sample magnetometer spectrum of the magnetic DOX-anchored nanogels and free SPION-$NH_2$ (e).

### 3.2. *In vitro* release

The release profiles were displayed in Figure 5. The release is strongly dependent on the GSH concentration. The relative release amount was utilized to express the release properties for easy comparison. Three GSH concentrations and two pHs were applied to assay the release features. The GSH levels in healthy cells, normal tissue or blood circulation are not at zero. The concentration of 2 μM was tested to investigate the release level for understanding of the potential toxicity in healthy tissues. The concentration of 10

mM was chosen so as to mimic the reduction potential in tumor intracellular environment.

The equilibrium release at pH 7.4 without GSH was 12% (orange line in Figure 5), whereas, the value reached around 17.8% at 2 μM GSH (green line in Figure 5). Theoretically, no DOX would be released if all DOX was covalently anchored onto alginate via disulfide bond. In practice, when attempted to prepare SA-SS-DOX, not modified DOX (free DOX) may be included in DOX-SH. Though we tried to remove the free DOX through dialysis against pH=5 aqueous medium and pure water, the free DOX is likely to combine SA with strong electrostatic attraction between the amino groups of DOX and the unmodified carboxyl groups of alginate and thus is hard to be removed out completely. In the release medium, PBS buffer (0.01M PBS) presented a salty environment, which is liable to trigger the release of this part of DOX inside the nanogel. Similar results were popularly observed in the similar structures.[36] Apparently this release is pretty low, meaning that the GSH level in healthy tissues would not cause obvious release. When GSH concentration reached 10 mM, the level in the tumor environment, MDAN-gel revealed 89% release (blue line in Figure 5). The test exhibited the typical GSH level-dependent release. The DOX was split away from the disulfide bond linkage under the scissor of reduction potential of GSH.

To note, at pH 5.5/GSH 10 mM, the nanogel exhibited an elevated release (red line in Figure 5) compared with the pH 7.4/GSH 10 mM. This is quick to be understood. Actually, the nanogel is fabricated via electrostatic assembly between the left carboxylic groups on SA and the amino groups on SPION. This type of linkage is acid sensitive and will be dissociated in acidic environment. After liberated from disulfide bonds under the GSH stimuli at neutral pH, DOX is still partially restricted within the nanogel. Only upon the disassembly of the nanogel under acidic environment, for instance, can DOX be completely released. Considering that the environment of lysosomes (pH 4.5-5.0), endosomes (pH 5.0-6.5) and cancerous tissues (pH 6.5-7.2) are more acidic than that of blood and normal tissues (pH 7.4),[37] this feature of release is advantageous for the specific release at tumor regions.

This kind of release profile will endow an effective release at targeted sites but a low leakage chance of DOX during the transportation to the targeted site and thus a low toxicity to normal tissue owing to the paucity of reduction environment in circulation or in normal tissue. These will be further verified in cell study and *in vivo* study.

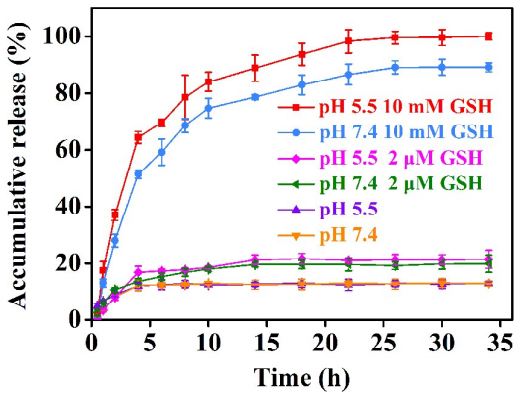

**Figure. 5.**The release of DOX from magnetic DOX-loaded nanogels dependent on pHs and GSH concentrations at 37°C.

### 3.4. Cell study

It is interesting to study the behavior of the nanogel in living cells. The cytotoxicity, cellular uptake and intracellular release behavior of MDAN-gel by HeLa cell line, in contrast with COS-7 cell line, were investigated.

#### 3.4.1. Cytotoxicity assay

The *in vitro* cytotoxicity of plain nanogel, free DOX, DOX-SH and MDAN-gel against both HeLa and COS-7 cells were assayed in contrast, shown in Figure 6. The $IC_{50}$ of MDAN-gel, free DOX and DOX-SH was estimated as 0.30 μg/mL, 0.18 μg/mL and 0.19 μg/mL, respectively, in Hela cells in terms of DOX amount (Figure 6a). That indicated that the thiolation of DOX did not affect DOX activity as anti-tumor therapeutics in that no significant difference was observed in terms of the $IC_{50}$ value. A little increase in $IC_{50}$ was observed in MDAN-gel. This is obvious because DOX was controlled to release. As a comparison, COS-7 cells demonstrated high tolerance to such a MDAN-gel. The $IC_{50}$ is even beyond the experimental upmost concentration, at least one order of magnitude higher than in Hela cells (Figure 6b). The selective activity on cancerous cells is presumably attributed to the result from the triggered release. Furthermore, plain nanogel was practically non-toxic up to a concentration of 20.6 μg/mL or 38.7 μg/mL, corresponding to Hela or COS-7 cells, respectively (Figure 6c), confirming that these materials used here have good biocompatibility and that the whole process for the preparation does not introduce any additional toxicity.

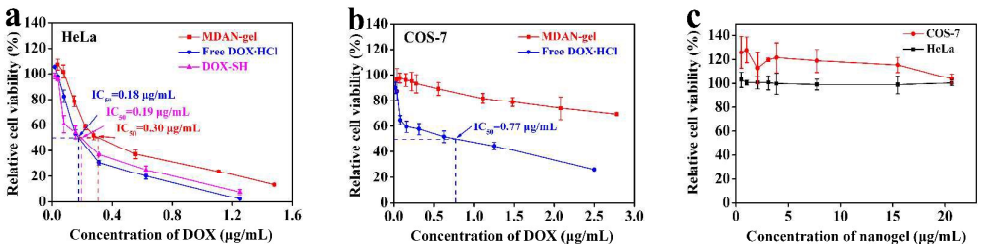


**Figure. 6.** Cytotoxicity in HeLa and COS-7 cells after 48 h incubation. Comparison among free DOX, DOX-SH and MDAN-gel in HeLa ( a ) and in COS-7 ( b ) or comparison of plain nanogel between in HeLa and in COS-7 ( c ). The standard deviation for each data point was averaged over eight samples.

#### 3.4.2. Cellular uptake and intracellular delivery

The cellular uptake and intracellular distribution of iron and DOX were evaluated with HeLa cells. Prussian blue staining provided a visual observation of the intracellular iron distribution, as shown in Figure 7. After incubated with plain magnetic nanogel for 24 h, HeLa cells were stained with potassium ferrocyanide and visualized with a reverse microscopy. The number of blue granules

significantly increased when the magnetic nanogel was applied, compared with the untreated group. This implies that the MDAN-gel could be rapidly endocytozed by HeLa cells.

A further study on the subcellular distribution and delivery behavior of the nanocarriers was observed by CLSM. As shown in Figure 8, HeLa cells were cultured with fluoresceinamine isomer labeled MDAN-gel for different time. Blue color is the cell nucleus treated with Hoechst 33258 and green and red colors are the fluorescence of fluoresceinamine and DOX, respectively. Kinetic CLSM observation matched the release profiles. After 4 h of incubation, the green and the red colors were both found in cytoplasm and coincided with each other, indicating the successful endocytosis of the nanocarrier. After 12 h of incubation, DOX could be identified around the cell nucleus. Whereas, strong red color of DOX was focused in the cell nuclei after 24 h. On the other hand, around 85% or 100% of DOX was released at 12 h or 24 h, respectively, in terms of the release profiles in Fig 5. The released DOX will enter the cell nuclei. The CLSM observation corroborates with the release profiles in Fig 5 in a time mode. Further, free DOX was explored in CLSM (fig.8e). It was found that free DOX entered nuclei within 4 h. As a comparison, strong red signal was observed in nuclei only after 24 h incubation, while the green color of the fluoresceinamine still distributed in the cytoplasm, implied that, as the incubation time prolonged, the cleavage of disulfide bond between DOX and alginate resulted into the release of DOX from the nanocarrier in the cytoplasm and the transfer of DOX into the nuclei. That is to say, the MDAN-gel could be internalized by cells and release DOX in the cytoplasm under the reducing intracellular environment. It is suggested that higher intracellular GSH concentration and more acidic environment accelerates the degradation of disulfide bonds and disassociation of electrostatic interaction as well as the intracellular DOX release from the nanogel and results in the rapid localization of DOX in the cell nucleus.

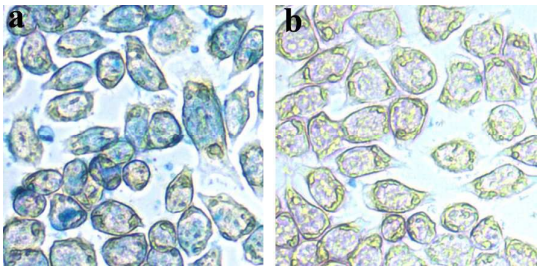


**Figure. 7.** Microscopic images of Prussian blue stained iron in HeLa cells treated by plain nanogels (a) in contrast with the untreated (b) . The images were obtained at 200× magnification.

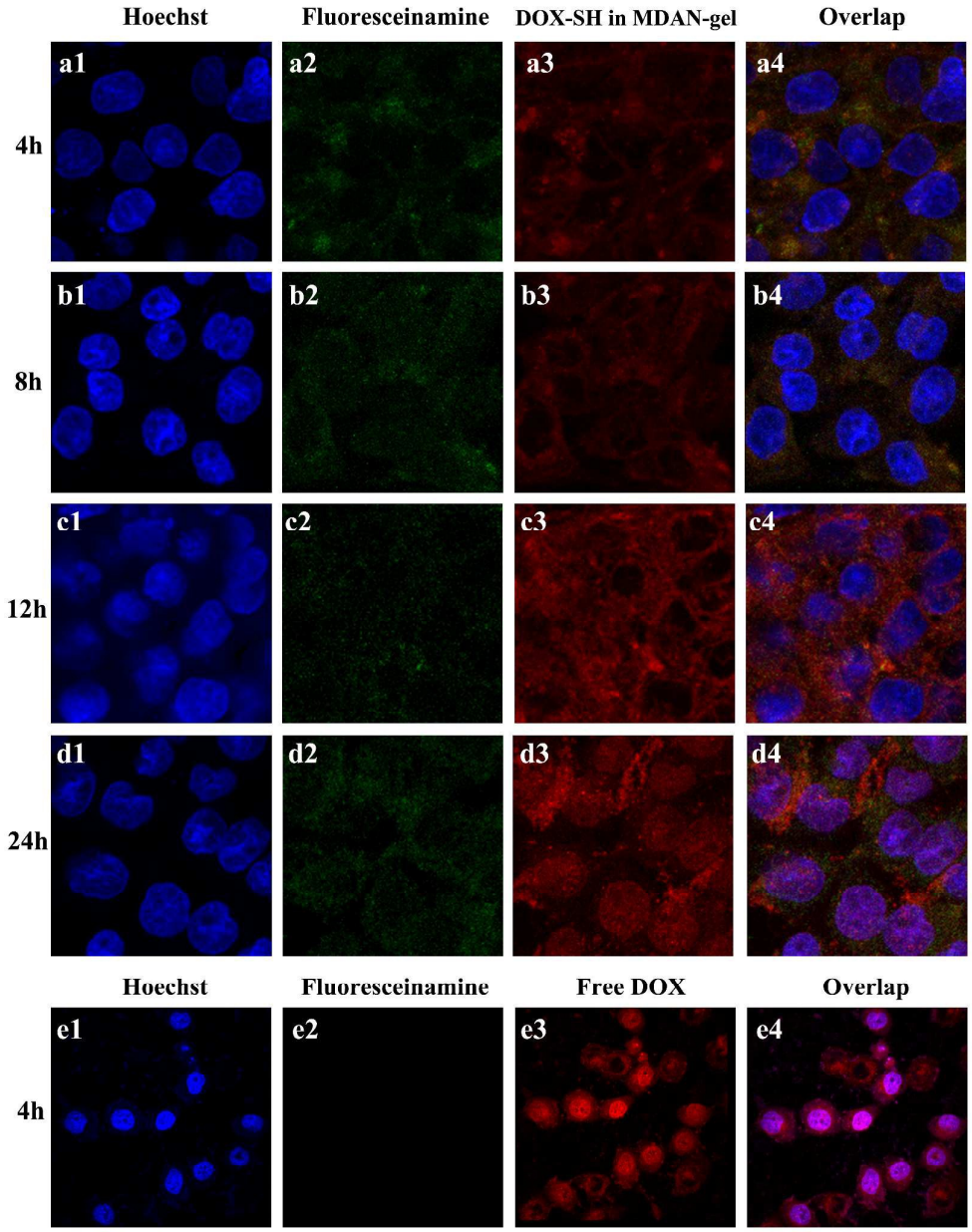


**Figure. 8.** Representative CLSM images of HeLa cells treated with free DOX for 4h and magnetic DOX-loaded nanogels for respective 4 h, 8 h, 12 h and 24 h. Blue is cell nucleus treated with Hoechst; Green is alginate treated with Fluoresceinamine; Red is the fluorescence of DOX-SH which released from MDAN-gel or free DOX; the last column is their overlap.

### 3.5. *In vivo* antitumor activity

The therapeutic efficacy of the nanogel was evaluated by monitoring the tumor growth and the body weight of mice, shown in Figure 9. Both the free DOX group and the MDAN-gel group displayed a strong inhibition to tumor growth. Figure 9a exhibits the images of tumors by different types of treatment. These images intuitively indicated the effective efficacy of the MADN-gel. Figure

9b is the quantitative results of the tumor sizes. The tumor was estimated at a volume of 477 $mm^3$ after 21-day treatment in the MDAN-gel group, with an inhibition rate of 80.7%, shown in Figure 9c. As a contrast, the free DOX treatment group displayed a bigger average size of 1442 $mm^3$ and a lower inhibition rate of 38.2%. Of course, PBS groups exhibited the largest tumor size. Since both of the free DOX group and the MADA-gel group were administrated with same DOX dose, the result revealed that the nanogel delivers more DOX to the targeted site and presents higher efficacy than DOX alone.

The change in body weight is usually taken as the index to evaluate the systemic toxicity.[28] As seen in Figure 9d, the mice in the nanogel treated group experienced slight weight loss on the first day, but was restored after two days. Afterwards, the mice had a stable growth in body weight and a healthy appearance throughout the entire experiment. In contrast, the free DOX treated group showed a large fluctuation range, and the lightest weight and the weakest activities were observed. This indicates the lower adverse effect in the MDAN-gel treated group than in the free DOX groups.

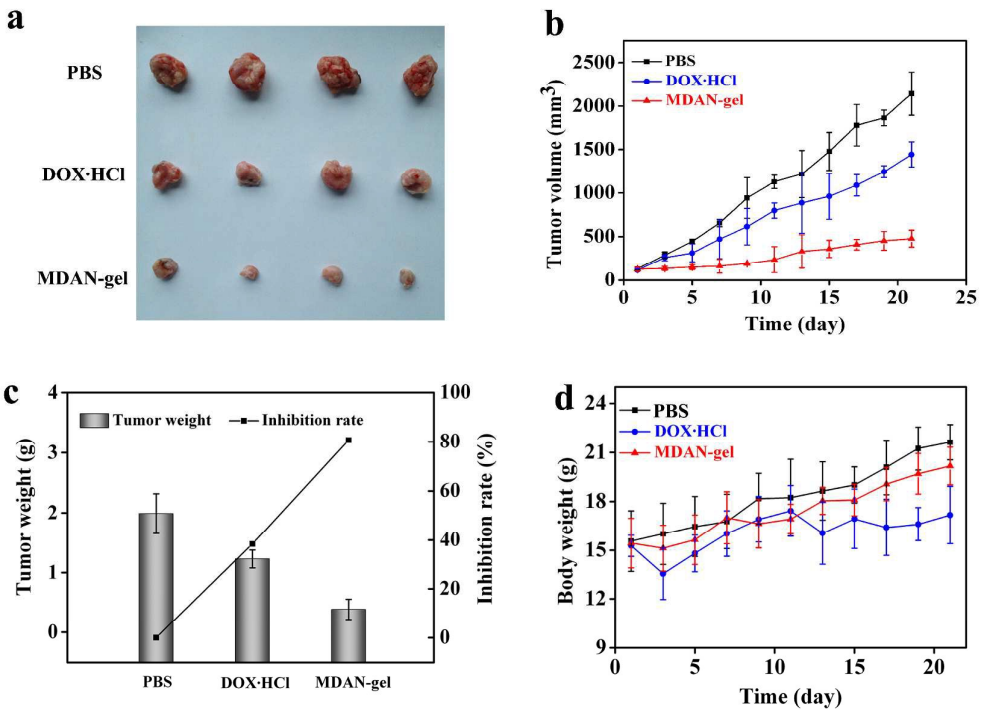


**Figure. 9.** The *in vivo* antitumor efficacy of the nanogel in BABL/c mice harboring H22 tumor. a) the representative tumors under different treatments, b) the tumor volume over the treatment regimen, c) the tumor weight at the experimental endpoint and the inhibition rate of tumor growth, and d) the change of body weight over the regimen.

### 3.6. Histological study

To confirm the antitumor efficacy induced by this targeted therapy, tumor sections were subjected to H&E staining (Figure 10). The tumors from the MDAN-gel or free DOX treated groups had increased areas with eosinophillic cytosol (pink) when compared to the control, the PBS treated group, indicating the induction of necrosis by drug treatment. Notably, MDAN-gel treatment induced more

remarkable necrosis in the tumors, which contained the most extensive necrotic centers and the least viable tumor cells. Conversely, more viable cells heterogeneously appeared throughout the whole tumor sections in the groups treated with free DOX than with MDAN-gel. This roughly exhibits that the nanogel presents high targeting effect, perhaps due to the fact that the nanogel can only be effectively triggered to release under the specific environments at the tumor site.

Additionally, as shown in Figure 11, treatments with MDAN-gel produced no apparent histological changes based on the tissue sections of liver, kidney, heart, lung and spleen in comparison with the PBS group. H&E staining of the liver tissues in PBS and MDAN-gel groups revealed normal hepatocytes, central veins, portal triads and liver lobules. In contrast, DOX induced significant degeneration and apoptosis of liver cells, expressing obvious hepatotoxicity. Normal Bowman's capsule, marked in red circle, surrounding glomeruli as well as convoluted tubules was observed in PBS and MDAN-gel groups, which is hardly to identify in the free DOX group. Thus serious nephrotoxicity in the free DOX group was demonstrated in kidney samples. It was well known that anthracyclines usually cause cardiotoxicity. Compared with the free DOX group, striated cardiac muscles with the centrally placed nucleus were observed in heart sections in the MDAN-gel group. Normal alveoli without the sign of pulmonary fibrosis were to find in the lung sections in the three groups, but significant pulmonary congestion was observed in the DOX group. No apparent difference was identified among the three groups in spleen samples. All above investigation indicated that the MDAN-gel behaves with the low toxicity as PBS or remarkably reduced toxicity in comparison of free DOX but higher therapy efficacy than free DOX.

Finally, the *in vivo* accumulation and distribution of the MDAD-gel were confirmed by Prussian blue staining, as shown in Figure 12. After the whole treatment, obvious accumulation of MDAN-gel (indicated in blue dots) was observed in the tumor tissue. This clearly confirms the effective targeting of the MDAN-gel or a high uptake in tumor. In vital organ sites, the staining results showed that the uptake of nanogel in liver, lung and spleen was greater than the uptake in heart and kidney. This result was in agreement with the previous literature.[38]

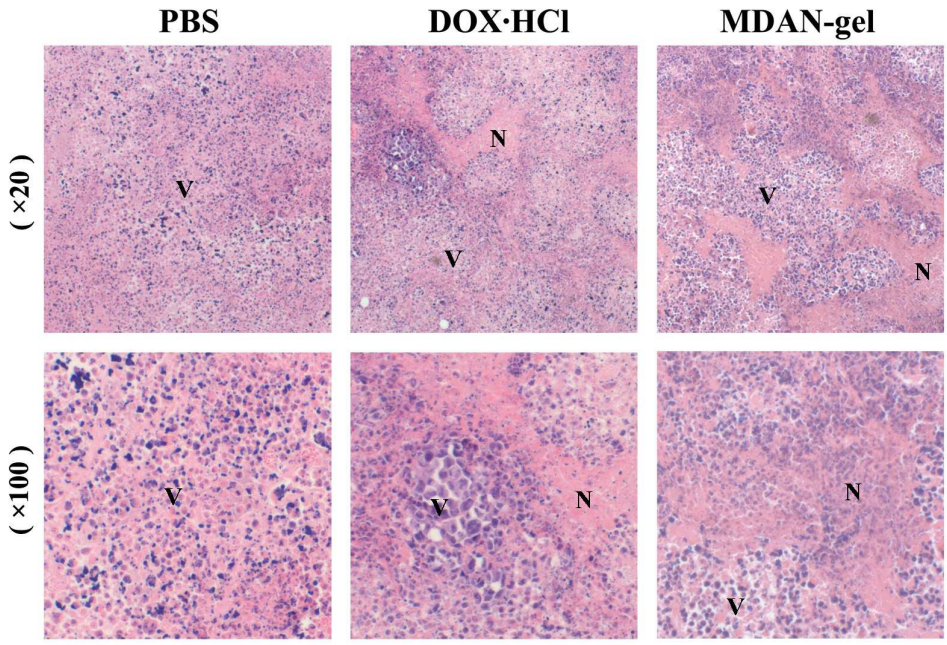


391

392 **Figure. 10.** Representative images of tumor sections for the confirmation of antitumor activity by H & E staining. Necrotic cells (N);

393 Viable cells (V).

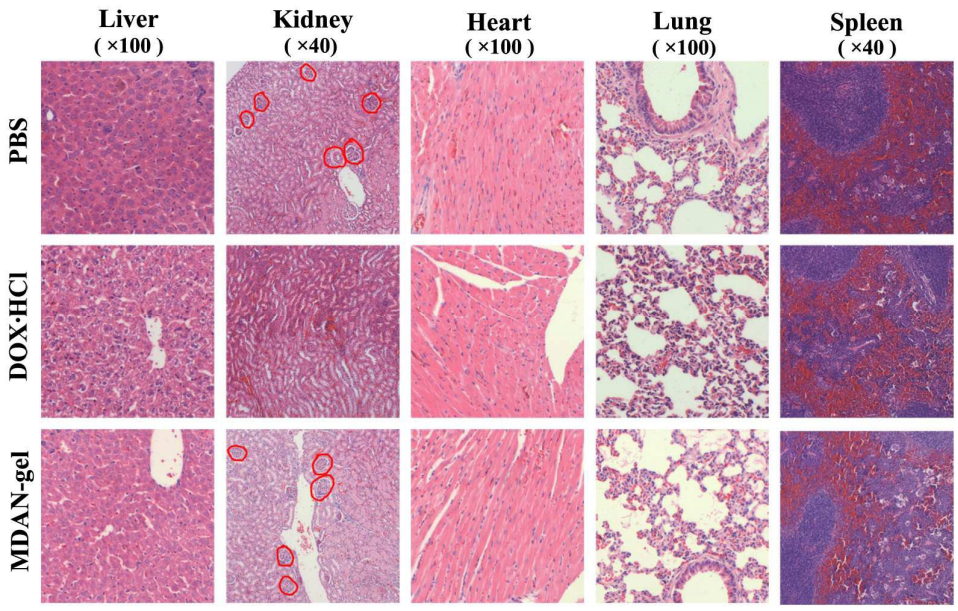


394

395 **Figure. 11.** Histologic examination of tissue sections of vital organs.

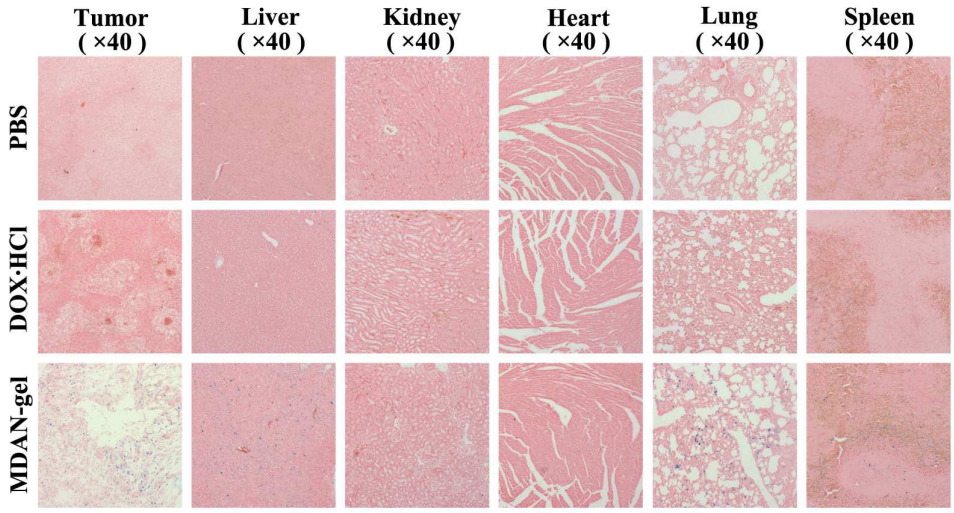


**Figure. 12.** *In vivo* Prussian blue staining showing the biodistribution of the nanogel in tumor tissue and vital tissues.

## 4. Discussion

The present goal is to pursue the high therapy efficacy and to minimize the adverse effect. Nanogels, usually a polymer-based crosslinked network, have attracted considerable attention due to their versatility in drug delivery systems.

DOX was fixed inside the nanogel through chemical conjugation to achieve the reduction-triggered release and to get rid of the leakage prior to arrival at targeting regions. The leakage most happens in the case of physical embedment of DOX. Cancerous cells and tissues offer the reduction environment. This kind of mechanism will noticeably reduce the release in the normal tissues and will allow high specific targeting release and efficient therapy with much low toxicity. This concept was confirmed by in vitro and *in vivo* tests here.

The release only reached 12% at pH 7.4 without GSH. The amount is believed to be far lower than the toxicity threshold if the total amount is administrated to meet the therapeutic requirement. This nanogel is thus a safe platform to deliver this kind of toxic therapeutics.

Besides, this fabrication is in a favor of the internalization of the MDAN-gel by cells and the release of DOX in the cytoplasm under the reducing intracellular environment. As a result, the intracellular DOX release from the nanogel accelerates the localization of DOX in the cell nucleus, enhancing the targeting efficiency. These have been verified in terms of the monitor of iron by Prussian blue staining and of the fluorescence images by CLSM. Interestingly, the MDAN-gel expresses intensive cytotoxicity to cancerous cell lines but high compatible with normal cell lines such as COS-7. The feature of selectivity of killing cancerous cells was further expressed in the effective therapy in tumor-bringing rats. *In vivo* experiments verified that the MDAN-gel has high therapeutic efficacy and low systemic toxicity.

In detail, upon the optimization of the ratio of thiolated SA to SPION, the nanogel was readily fabricated via their electrostatic interaction in an appropriate size and with high negative surface charge for the assurance of high storage stability. Alginate was

chosen as the primary material for the fabrication of the nanogel in that it possesses the features of hydrophilicity, biocompatibility, non-toxicity, and low immunogenicity[39]. Other than that, alginate provides plentiful carboxylic groups, which present a number of benefits in the fabrication of the nanogel. The degree of thiolation of alginate was 12.5%, as above. Clearly, the thiol groups were to chemically conjugate with DOX via disulfide bond linkage for reduction responsiveness of drug release. In another word, 87.5% carboxylic groups are exclusive of thiolation. The carboxylic groups left were utilized for subsequent combination with SPION-$NH_2$ via electrostatic interaction. The electrostatic combination endows the nanogel the acid responsiveness of release. Moreover, there are still partial carboxylic groups which provide the nanogel for the negative surface charge, essential for the stability in storage. To be honest, we attempted to create carboxylic groups onto dextran. Regretted, due to only a limited number of carboxylic groups created on the dextran molecule, the DEE was very low and the reduction responsiveness was too weak to be meaningful for further investigation. Therefore the plentiful carboxylic groups are basically required for this kind of fabrication.

In our previous researches, polymer coated MNPs could not only obviously yield distinctive magnetic resonance imaging (MRI) of the brain tumor in a rat model[40] but also enhance the magnetophoretic mobility for high magnetic targeting[41]. After that, we explored the apical to basolateral transport of magnetic nanoparticles across the cell monolayer by pulsing the magnetic field[4]. Combined with other literatures, MNPs were incorporated as well into the nanogel as the source of the magnetic properties with a couple benefits, such as active targeting[42], MRI[6] and induced hyperthermia treatment.[43] These features are well known and widely investigated elsewhere, though, not involved in this study. Additionally, the manipulation of the superparamagnetic nanogel is facile and repeatable.

*In vivo* studies revealed the MDAN-gel presents higher effective efficacy than free DOX with as low systemic adverse effect as PBS. These studies further endorse the hypothesis in the design of the vehicle, as anticipated.

## 5. Conclusion

We have demonstrated a superparamagnetic nanogel with the reduction-triggered feature based on the linkage of chemical bond. An appropriate size of the nanogel with high surface negative charge was achieved through the optimized conditions. Alginate was chosen due to its affluent carboxylic groups. SPION was utilized in favor of its magnetic targeting, high biocompatibility, hyperthermia, enhancement in MRI etc. The nanogel expresses the release behaviors a typical reduction-triggered release manner, preferring releasing DOX in the cancerous environment. By virtue of the chemical conjugation, the release of DOX was found to intensively restrain at normal environment such as at pH 7.4 without GSH applied. Cellular uptake test and CLSM images indicated a fantastic selectivity of killing cancerous cells and a fast internalization of the nanogel and efficient intracellular drug delivery, principally in the nucleus. *In vivo* studies indicates high therapeutic efficacy with high targeting release and low systemic adverse effect. All these experiments certified that the present nanogel provides a promising platform for tumor therapy with high targeting efficiency and low system adverse effect.

## Acknowledgments

This research was supported by the National Natural Science Foundation of China (21571147), as well as by the Program of Hubei Provincial Department of Education, China (Q20151518), by Innovative Team Program of Natural Science Foundation of Hubei Province (2014CFA011), by Innovative Team Incubation Program in High-tech Industry of Wuhan City (2014070504020244), and by the Scientific Research Foundation of Wuhan Institute of Technology (10125032).

## References

(1) B. Felice, M. P. Prabhakaran, A. P. Rodríguez and S. Ramakrishna, *Mat. Sci. Eng. C*, 2014, **41**, 178-195.

(2) S. Mura, J. Nicolas and P. Couvreur, *Nat. Mater.*, 2013, **12**, 991-1003.

(3) R. Cheng, F. Meng, C. Deng, H.A. Klok and Z. Zhong, *Biomaterials*, 2013, **34**, 3647-3657.

(4) K. A. Min, M. C. Shin, F. Yu, M. Yang, A. E. David, V. C. Yang and G. R. Rosania, *ACS nano*, 2013, **7**, 2161-2171.

(5) M. Domenech, I. Marrero-Berrios, M. Torres-Lugo and C. Rinaldi, *ACS nano*, 2013, **7**, 5091-5101.

(6) A. Curcio, R. Marotta, A. Riedinger, D. Palumberi, A. Falqui and T. Pellegrino, *Chem. Commun.*, 2012, **48**, 2400-2402.

(7) C. Tassa, S. Y. Shaw and R. Weissleder, *Accounts. Chem. Res.*, 2011, **44**, 842-852.

(8) R. Cheng, F. Feng, F. Meng, C. Deng, J. Feijen and Z. Zhong, *J. Control. Release*, 2011, **152**, 2-12.

(9) Z.Y. Li, J.J. Hu, Q. Xu, S. Chen, H.Z. Jia, Y.X. Sun, R.X. Zhuo and X.Z. Zhang, *J. Mater. Chem. B* 2015, **3**, 39-44.

(10) D. Yang, W. Chen and J. Hu, *J. Phys. Chem. B*, 2014, **118**, 12311-12317.

(11) X. Zhang, K. Achazi, D. Steinhilber, F. Kratz, J. Dernedde and R. Haag, *J. Control. Release*, 2014, **174**, 209-216.

(12) Y. Zhan, M. Gonçalves, P. Yi, D. Capelo, Y. Zhang, J. Rodrigues, C. Liu, H. Tomás, Y. Li and P. He, *J. Mater.Chem. B*, 2015.

(13) Y. Shen, X. Fu, W. Fu and Z. Li, *Chem. Soc. Rev.*, 2014, **44**, 612-622.

(14) Q. Yang, L. Tan, C. He, B. Liu, Y. Xu, Z. Zhu, Z. Shao, B. Gong and Y.M. Shen, *Acta Biomater.*, 2015, **17**, 193-200.

(15) E. Pérez, A. Fernández, R. Olmo, J. M. Teijón and M. D. Blanco, *Colloid. Surface. B*, 2014, **116**, 247-256.

(16) P. Gou, W. Liu, W. Mao, J. Tang, Y. Shen and M. Sui, *J. Mater. Chem. B*, 2013, **1**, 284-292.

(17) V. T. Huynh, J. Y. Quek, P. L. de Souza and M. H. Stenzel, *Biomacromolecules*, 2012, **13**, 1010-1023.

(18) F. Greco, I. Arif, R. Botting, C. Fante, L. Quintieri, C. Clementi, O. Schiavon and G. Pasut, *Polym. Chem.-UK*, 2013, **4**, 1600-1609.

(19) M. Bio, G. Nkepang and Y. You, *Chem. Commun.*, 2012, **48**, 6517-6519.

(20) J. Huang, Y. Xue, N. Cai, H. Zhang, K. Wen, X. Luo, S. Long and F. Yu, *Mat. Sci. Eng. C*, 2015, **46**, 41-51.

(21) J. Chen, M. Shi, P. Liu, A. Ko, W. Zhong, W. Liao and M. M. Xing, *Biomaterials*, 2014, **35**, 1240-1248.

(22) F. Yu, Y. Huang, A. J. Cole and V. C. Yang, *Biomaterials*, 2009, **30**, 4716-4722.

(23) H. Zhang, Y. Xue, J. Huang, X. Xia, M. Song, K. Wen, X. Zhang, X. Luo, N. Cai and S. Long, *J. Mater. Sci.*, 2015, **50**, 1-14.

(24) M. Davidovich-Pinhas, O. Harari and H. Bianco-Peled, *J. Control. Release*, 2009, **136**, 38-44.

(25) K. Kafedjiiski, A. H. Krauland, M. H. Hoffer and A. Bernkop-Schnürch, *Biomaterials*, 2005, **26**, 819-826.

(26) B. L. Strand, Y. A. Mørch, T. Espevik and G. Skjåk-Bræk, *Biotechnol. Bioeng.*, 2003, **82**, 386-394.

(27) A. Shalviri, G. Raval, P. Prasad, C. Chan, Q. Liu, H. Heerklotz, A. M. Rauth and X. Y. Wu, *Eur. J. Pharm. Biopharm.* 2012, **82**, 587-597.

(28) C. Zhang, W. Wang, T. Liu, Y. Wu, H. Guo, P. Wang, Q. Tian, Y. Wang and Z. Yuan, *Biomaterials*, 2012, **33**, 2187-2196.

(29) C. Hwang, A. J. Sinskey and H. F. Lodish, *Science*, 1992, **257**, 1496-1502.

(30) S. Santra, C. Kaittanis, O. J. Santiesteban and J. M. Perez, *J. Am. Chem. Soc.*, 2011, **133**, 16680-16688.

(31) X. Zhang, L. Meng, Q. Lu, Z. Fei and P. J. Dyson, *Biomaterials*, 2009, **30**, 6041-6047.

(32) Z. Durmus, H. Kavas, M. S. Toprak, A. Baykal, T. G. Altınçekiç, A. Aslan, A. Bozkurt and S. Coşgun, *J. Alloy. Compd.*, 2009, **484**, 371-376.

(33) S. Kayal and R. Ramanujan, *Mat. Sci. Eng. C*, 2010, **30**, 484-490.

(34) J. Fang, H. Nakamura and H. Maeda, *Adv. Drug Deliver. Rev.*, 2011, **63**, 136-151.

(35) G. Ajay Kumar and G. Mona, *Biomaterials*, 2005, **26**, 3995-4021.

(36) M. H. Lee, J. Y. Kim, J. H. Han, S. Bhuniya, J. Sessler, C.Kang, J. S. Kim, *J. Am. Chem. Soc.*, 2012, **134**, 12668-12674.

(37) J.Z. Du, X.J. Du, C.Q. Mao and J. Wang, *J. Am. Chem. Soc.*, 2011, **133**, 17560-17563.

(38) Z. Tang, D. Li, H. Sun, X. Guo, Y. Chen and S. Zhou, *Biomaterials*, 2014, **35**, 8015-8027.

(39) W. R. Gombotz and S. F. Wee, *Adv. Drug Deliver. Rev.*, 2012, **64**, 194-205.

(40) B. Chertok, B. A. Moffat, A. E. David, F. Yu, C. Bergemann, B. D. Ross and V. C. Yang, *Biomaterials*, 2008, **29**, : 487–496.

(41) F. Yu, L. Zhang, Y. Huang, K. Sun, A. E. David and V. C. Yang, *Biomaterials*, 2010, **31**, 5842-5848.

(42) Z. Zhao, D. Huang, Z. Yin, X. Chi, X. Wang and J. Gao, *J. Mater. Chem.*, 2012, **22**, 15717-15725.

(43) M. Guo, Y. Yan, X. Liu, H. Yan, K. Liu, H. Zhang and Y. Cao, *Nanoscale*, 2010, **2**, 434-441.